Fault-Tolerant Homopolar Magnetic Bearings

Ming-Hsiu Li, Alan B. Palazzolo, Andrew Kenny, Andrew J. Provenza, Raymond F. Beach, and Albert F. Kascak

***Abstract*—This paper summarizes the development of a novel magnetic suspension that improves reliability via fault-tolerant operation. The suspension is suitable for flywheels used in satellites and space stations for attitude control and energy storage. Specifically, we show that flux coupling between poles of a homopolar magnetic bearing can deliver desired forces even after termination of coil currents to a subset of "failed poles." Linear, coordinate-decoupled force-voltage relations are also maintained before and after failure by bias linearization. We determined current distribution matrices that adjust the currents and fluxes following a pole set failure for many faulted pole combinations. We used one-dimensional magnetic circuit models with fringe and leakage factors derived from detailed, three-dimensional finite-element field models to obtain the current distribution matrices and the system response. Reliability is based on the success criterion that catcher bearing-shaft contact does not occur after pole failures. The magnetic bearing reliability is improved by increasing the number of the radial poles. An advantage of our method over other redundant approaches is a significantly reduced requirement for backup hardware such as additional actuators or power amplifiers.**

***Index Terms*—Fault-tolerant control, homopolar, magnetic bearings, magnetic suspensions, reliability.**

List of Acronyms

ACESE	Attitude control energy storage experiment.
CB	Catcher bearing.
CDM	Current distribution matrix.
CG	Center of gravity (mass).
FTC	Fault-tolerant control.
HCB	Homopolar combo bearing (combo bearing).
HEMB	Heteropolar magnetic bearing.
HOMB	Homopolar magnetic bearing.
HRB	Homopolar radial bearing (radial bearing).
ISS	International space station.
MB	Magnetic bearing.
PA	Power amplifier.
PM	Permanent magnet.

Nomenclature

a'	Axial pole face area of HCB.
a_d	Dead pole face area of HRB.
a_i	Face area of the ith pole of HRB and HCB.
C_e, C_c	Housing support system damping, CB contact damping.
e	Flywheel eccentricity.
F_n	Normal force of CB.
g_i	Air gap of the ith pole of HRB and HCB.
g_{0d}	Air gap of dead pole of HRB.
$H_{\rm pm}$	Coercive force of PM.
$I_{\rm tr}$, $I_{\rm pr}$	Rotor transverse and polar moment of inertia.
I_{t1h}, I_{t2_h}	Housing transverse moment of inertia.
i_j	Current of the jth power amplifier of HRB and HCB.
K_e, K_c	Housing support system stiffness, CB contact stiffness.
K_{v1}, K_{v2}, K_{v3}	desired control voltage stiffness for X_1, X_2, X_3.
$L_{\rm pm}$	Length of permanent magnet.
M_h, M_r	Mass of housing, mass of rotor.
$L^{(\ )}_{(\ )(\ )}$	Distance from the rotor and housing CG to components (or disturbance). Superscript: A or B for components at end A or B. First subscript: b for MB, c for CB, s for sensor, e for housing support, and d for disturbance. Second subscript: r for rotor and h for housing.
N_i	Number of turns on the ith coil of HRB and HCB.
N_{c1}, N_{c2}, N_{c3}	Number of turns on decoupling chokes.
$\Re_{c1}$, $\Re_{c2}$	Air-gap reluctance of decoupling chokes.
$\Re_{pm}$	Reluctance of PM.
θ_i	Angle of the ith radial pole of HRB and HCB.
μ	Dynamic friction coefficient of CB.
μ_0	Permeability of free space
ϕ_i	Flux of the ith pole of HRB and HCB.
ω	Rotor angular velocity.
φ	Contact angle of CB.
ψ	Phase angle of mass unbalance force.

Manuscript received July 10, 2003; revised June 12, 2004. This work was supported by NASA Glenn (NRA-GRC-99-01) and the NASA Center for Space Power (CSP) at Texas A&M.

M.-H. Li is at 1 Hensel Dr. Apt. #X4I, College Station, TX 77840 USA (e-mail: Li4286@neo.tamu.edu).

A. B. Palazzolo and A. Kenny are with the Department of Mechanical Engineering, Texas A&M University, College Station, TX 77843-3123 USA (e-mail: a-palazzolo@tamu.edu; a-kenny@tamu.edu).

A. J. Provenza, R. F. Beach, and A. F. Kascak are at 21000 Brookpark Road, Cleveland, OH 44135 USA (e-mail: Andrew.J.Provenza@gr.nsas.gov; Raymond.F.Beach@gr.nsas.gov; Albert.F.Kascak@gr.nsas.gov).

Digital Object Identifier 10.1109/TMAG.2004.833428

I. Introduction

ATTRACTIVE magnetic bearing actuators as shown in Fig. 1 possess individual pole forces that vary quadratically with current. The net force of the bearing may be linearized with respect to the control voltages by utilizing a bias flux component [1], [2]. Thus, the X_1, X_2, and X_3 forces become decoupled, i.e., dependent only on their respective control voltages (V_{c1}, V_{c2} and V_{c3}). Maslen and Meeker [3]

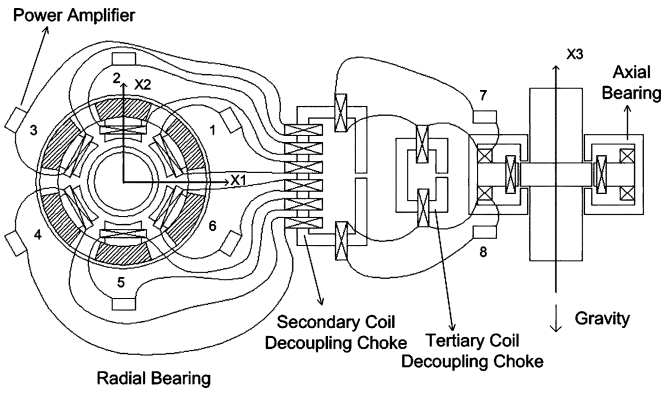

Fig. 1. Six-pole homopolar combo bearing.

provided a generalization of this approach for heteropolar magnetic bearings (HEMB), which derive their bias flux from electric coils and utilize both N and S at different poles.

Fault-tolerant control (FTC) of HEMBs has been demonstrated on a five-axis, flexible rotor test rig with three CPU failures and two (out of eight) adjacent coil failures [4]. Current distribution matrices (CDM) for HEMBs were extended to cover five pole failures out of eight poles [5], [6] and for the case of significant effects of material path reluctance and fringing [7].

The fault-tolerant approach outlined above utilizes a CDM that changes the current in each pole after failure in order to achieve linearized, decoupled relations between control forces and control voltages. A failure configuration is defined by the subset of poles that fail due either to shorting of a turn in a coil or to failure of a power amplifier. In general, there exist (2^n-1) number of possible failure configurations for an n pole magnetic bearing.

A unique contribution of the present work includes the extension of a CDM approach to four-, six-, and seven-pole homopolar magnetic bearings (HOMBs). The HOMB commonly uses permanent magnets (PMs) for its bias flux to increase the actuator's efficiency and reduce heat generation [8]. Points on the surface of the spinning journal in the homopolar bearing do not experience north-south flux reversals thereby reducing rotor losses due to hysteresis and eddy currents.

A second contribution of the present work is an investigation of the reliabilities of fault-tolerant HOMB. The reliabilities presented are system specific for two reasons. 1) An exact solution CDM may not exist for certain pole failure configurations. An approximate solution will always exist though and its effectiveness is evaluated via failure simulation for the specific system studied. 2) The success criterion is defined by: no contact between the shaft and catcher bearings during the failure and CDM implementation sequence. Satisfaction of this criterion will depend on the system studied and the delay time τ_d required to identify which poles have failed, to turn off the power amplifiers for these poles and to implement the corresponding CDM for the remaining poles.

The specific system employed for this study is a high speed flywheel under development for energy storage and attitude control applications on satellites or on the international space station (ISS). A general result identified from the study is an increase in reliability as the number of poles increase.

This paper is organized as follows. Section II presents the FTC algorithm including the requirements of FTC, the CDMs of HCBs and HRBs, and decoupling chokes. Section III develops the flywheel and magnetic suspension dynamics model. Section IV provides examples of FTC operation. Section V shows the reliability of magnetic bearings based on FTC operation. Finally, Section VI summarizes some interesting trends of the HOMBs and the advantages over the HEMBs. The future of this research direction is also discussed in this section.

II. Fault-Tolerant Control

A. Requirements

Derivation of the FTC approach requires applications of Ampere's, Ohm's, and Faraday's laws, and the Maxwell stress tensor to the multipath magnetic circuit in a magnetic bearing. The physical requirements of FTC include the following.

1) *Decoupling Condition:* The x_i control voltage does not affect the x_j control force unless $i = j$, where the triple $(x_1\ x_2\ x_3)$ is the Cartesian coordinate.
2) *Linearity Condition:* The x_i control voltage and x_i control force are linearly related.
3) *Invariance Condition 1:* The force/voltage gains are not affected by the failure.
4) *Invariance Condition 2:* The force/position gains are not affected by the failure.

The FTC requirement 4) is automatically satisfied for a magnetic bearing with bias fluxes generated by permanent magnets located circumferentially and in equal space. This results since the permanent magnets and the resulting bias flux are unaffected by the failure state of the poles.

A complete derivation of the FTC theory is developed next for a six-pole homopolar combination (combo, radial and axial forces) magnetic bearing. The FTC theory for the four- and seven-pole bearings is very similar and is not included.

B. Six-Pole Homopolar Combo Bearing (HCB)

Fig. 1 depicts a combination (radial/axial) six-pole HCB installed on a vertically directed shaft. The actuator has six radial poles and coils and two axial poles and coils. The axial coils are wound circumferentially around the shaft and the radial coils are wound around the poles. The coil leads also form secondary coils around a common decoupling choke and the axial leads also form tertiary coils around a second decoupling choke. The decoupling chokes eliminate mutual inductances and ensure that the inductance matrix is nonsingular, which ensures electric circuit stability [2]. The laminated construction provides for an accurate approximation of infinite bandwidth between currents and fluxes. Following common practice, the actuator is modeled as an equivalent magnetic circuit with derated magnetic strength accounting for leakage and derated gap flux density to account for fringing. Fig. 2 shows the six-flux paths through the radial poles and two-flux paths through the axial poles.

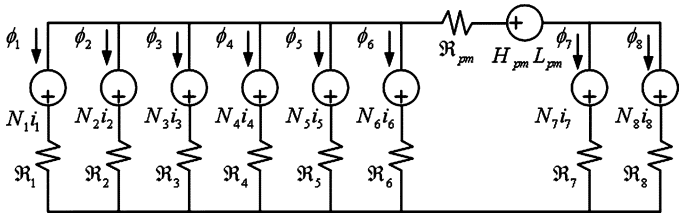

Fig. 2. Equivalent magnetic circuit for the six-pole homopolar combo bearing.

The magnetic circuit provides a useful tool to present flux conservation and Ampere law relations with an equivalent electric circuit model. Kirchhoff's law applied to Fig. 2 yields

$$\begin{bmatrix} \Re_1 & -\Re_2 & 0 & 0 & 0 & 0 & 0 & 0 \\ 0 & \Re_2 & -\Re_3 & 0 & 0 & 0 & 0 & 0 \\ 0 & 0 & \Re_3 & -\Re_4 & 0 & 0 & 0 & 0 \\ 0 & 0 & 0 & \Re_4 & -\Re_5 & 0 & 0 & 0 \\ 0 & 0 & 0 & 0 & \Re_5 & -\Re_6 & 0 & 0 \\ \Re_{pm} & \Re_{pm} & \Re_{pm} & \Re_{pm} & \Re_{pm} & \Re_{pm}+\Re_6 & -\Re_7 & 0 \\ 0 & 0 & 0 & 0 & 0 & 0 & \Re_7 & -\Re_8 \\ 1 & 1 & 1 & 1 & 1 & 1 & 1 & 1 \end{bmatrix} \begin{bmatrix} \phi_1 \\ \phi_2 \\ \phi_3 \\ \phi_4 \\ \phi_5 \\ \phi_6 \\ \phi_7 \\ \phi_8 \end{bmatrix}$$

$$= \begin{bmatrix} N_1 & -N_2 & 0 & 0 & 0 & 0 & 0 & 0 \\ 0 & N_2 & -N_3 & 0 & 0 & 0 & 0 & 0 \\ 0 & 0 & N_3 & -N_4 & 0 & 0 & 0 & 0 \\ 0 & 0 & 0 & N_4 & -N_5 & 0 & 0 & 0 \\ 0 & 0 & 0 & 0 & N_5 & -N_6 & 0 & 0 \\ 0 & 0 & 0 & 0 & 0 & N_6 & -N_7 & 0 \\ 0 & 0 & 0 & 0 & 0 & 0 & N_7 & -N_8 \\ 0 & 0 & 0 & 0 & 0 & 0 & 0 & 0 \end{bmatrix} \begin{bmatrix} i_1 \\ i_2 \\ i_3 \\ i_4 \\ i_5 \\ i_6 \\ i_7 \\ i_8 \end{bmatrix}$$

$$+ \begin{bmatrix} 0 \\ 0 \\ 0 \\ 0 \\ 0 \\ H_{pm}L_{pm} \\ 0 \\ 0 \end{bmatrix} \qquad R\Phi = NI + H \tag{1}$$

where

$$\Re_i = \frac{g_i}{(\mu_0 a_i)}. \tag{2}$$

Let A represent a diagonal matrix of pole gap areas then by assuming uniform flux densities in each gap

$$AB = \Phi. \tag{3}$$

Substituting (3) into (1) yields

$$B = VI + B_{\text{bias}} \tag{4}$$

where

$$V = A^{-1}R^{-1}N \tag{5}$$

$$B_{\text{bias}} = A^{-1}R^{-1}H. \tag{6}$$

Equations (4)–(6) show that the control flux (VI) varies with control current and with shaft position (gap values); however, the bias flux (B_{bias}) varies solely with shaft position.

Magnetic bearings typically utilize servo power amplifiers (PA) that provide 1.2–2.0 kHz bandwidth for inductive loads ranging between 2 and 8 mH. Thus, it is acceptable to use a constant for the control current per control voltage gain. Let

$$V_c = (V_{c1}\ V_{c2}\ V_{c3})^T \tag{7}$$

represent the control voltages and the matrix T is the CDM. Then in the absence of pole failures

$$I' = TV_c \tag{8}$$

where T includes the PA gain and the current distribution terms. Fault conditions are represented using the matrix K that has a null row for each faulted pole. Then the failed actuator control currents become

$$I = KI' = KTV_c. \tag{9}$$

For example, if coils 1 and 2 fail

$$K = \text{diag}(0\ 0\ 1\ 1\ 1\ 1\ 1\ 1). \tag{10}$$

The magnetic forces are determined from the Maxwell stress tensor as

$$F_j = B^T\gamma_j B \tag{11}$$

where γ_j are 8×8 matrices and given as

$$\gamma_1 = \text{diag}\left[\frac{a_i \cos\theta_i}{(2\mu_0)}\right], \quad i = 1 \sim 6$$
$$\gamma_1(7,7) = \gamma_1(8,8) = 0 \tag{12}$$

$$\gamma_2 = \text{diag}\left[\frac{a_i \sin\theta_i}{(2\mu_0)}\right], \quad i = 1 \sim 6$$
$$\gamma_2(7,7) = \gamma_2(8,8) = 0 \tag{13}$$

$$\gamma_3(7,7) = -\gamma_3(8,8) = \frac{a'}{(2\mu_0)}$$
$$\text{all other components are zero.} \tag{14}$$

Substitute (9) into (4)

$$B = WV_c + B_{\text{bias}} \tag{15}$$

where $W = VKT$. The magnetic forces are given in terms of control voltages and bias flux density as

$$F_j = V_c^T W^T \gamma_j W V_c + 2B_{\text{bias}}^T \gamma_j W V_c + B_{\text{bias}}^T \gamma_j B_{\text{bias}} \tag{16}$$

where $j = 1, 2$, and 3. The magnetic forces are proportional to the square of control voltages in (16). The following constraint equations must be satisfied in order to meet FTC requirements (a), (b), and (c)

$$W^T\gamma_1 W = 0_{3\times 3} \tag{17}$$

$$2B_{\text{bias}}^T\gamma_1 W = [K_{v1}\ 0\ 0] \tag{18}$$
$$W^T\gamma_2 W = 0_{3\times 3} \tag{19}$$
$$2B_{\text{bias}}^T\gamma_2 W = [0\ K_{v2}\ 0] \tag{20}$$
$$W^T\gamma_3 W = 0_{3\times 3} \tag{21}$$
$$2B_{\text{bias}}^T\gamma_3 W = [0\ 0\ K_{v3}]. \tag{22}$$

Equations (17) to (22) are 18 nonlinear and nine linear algebraic equations for the CDM entries, t_{ij}. The CDM entries are obtained by requiring simultaneous solution of these constraint equations, and minimization of the Frobenius matrix norm of the CDM. This is typically performed at the magnetic center, i.e., the location where the bias flux balances the static loads on the bearing. The norm of the current vector, I in (9), satisfies the consistency condition [9]

$$\|I\| \le \|K\| \cdot \|T\| \cdot \|V_c\| \tag{23}$$

where for a Frobenius norm

$$\|K\| = \sqrt{\sum_{i,j} K_{ij}^2} \tag{24}$$
$$\|T\| = \sqrt{\sum_{i,j} t_{ij}^2} \tag{25}$$
$$\|V_c\| = \sqrt{\sum_{i} V_{ci}^2}. \tag{26}$$

Thus, by (23), reduction of $\|I\|$ follows from minimizing $\|T\|$. The Lagrange multiplier approach is employed to locate a solution of the equations in (17) to (22), that minimize $\|T\|$. The cost function is

$$L = \sum_{i=1}^{p}\sum_{j=1}^{3} t_{ij}^2 + \sum_{k=1}^{27}\lambda_k h_k \tag{27}$$

where p is the number of functioning poles, λ_k are the Lagrange multipliers and h_k are the 27 constraint equations. The solution condition is

$$\frac{\partial L}{\partial Z_m} = 0, \quad Z_m \in \{t_{ij}, \lambda_k\} \tag{28}$$

which implies

$$F(t_{ij},\lambda_k) = \left[h_1\ \cdots\ h_{27}\ \frac{\partial L}{\partial t_{11}}\ \frac{\partial L}{\partial t_{12}}\ \frac{\partial L}{\partial t_{13}}\ \cdots\ \frac{\partial L}{\partial t_{p1}}\ \frac{\partial L}{\partial t_{p2}}\ \frac{\partial L}{\partial t_{p3}}\right]^T = 0. \tag{29}$$

For the six-pole HCB, the total set of equations is overdetermined, i.e., more equations than unknowns (at most 24 unknowns), therefore a solution exists only in the least square sense. The nonlinear equation, least square based solver available in MATLAB is employed for this purpose. The effectiveness of each solution in satisfying the FTC requirements must be checked by transient response simulation of the respective fault event since the least square solution is not exact.

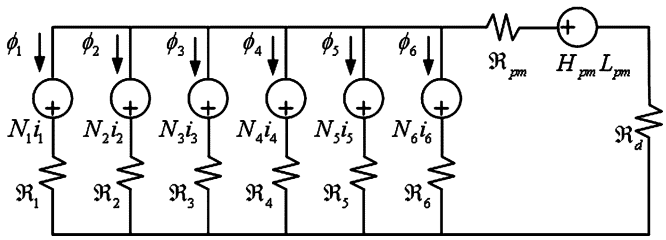

Fig. 3. Equivalent magnetic circuit for the six-pole homopolar radial bearing.

C. Six-Pole Homopolar Radial Bearing (HRB)

The six-pole HRB provides force solely in the two transverse (radial) directions. A magnetic circuit model for this bearing is illustrated in Fig. 3. The flux-current relations for this circuit are obtained by applying Kirchoff's laws, which yield

$$\begin{bmatrix} \Re_1 & -\Re_2 & 0 & 0 & 0 & 0 \\ 0 & \Re_2 & -\Re_3 & 0 & 0 & 0 \\ 0 & 0 & \Re_3 & -\Re_4 & 0 & 0 \\ 0 & 0 & 0 & \Re_4 & -\Re_5 & 0 \\ 0 & 0 & 0 & 0 & \Re_5 & -\Re_6 \\ \Re_d+\Re_{pm} & \Re_d+\Re_{pm} & \Re_d+\Re_{pm} & \Re_d+\Re_{pm} & \Re_d+\Re_{pm} & \Re_d+\Re_{pm}+\Re_6 \end{bmatrix}$$
$$\begin{bmatrix}\phi_1\\ \phi_2\\ \phi_3\\ \phi_4\\ \phi_5\\ \phi_6\end{bmatrix} = \begin{bmatrix} N_1 & -N_2 & 0 & 0 & 0 & 0 \\ 0 & N_2 & -N_3 & 0 & 0 & 0 \\ 0 & 0 & N_3 & -N_4 & 0 & 0 \\ 0 & 0 & 0 & N_4 & -N_5 & 0 \\ 0 & 0 & 0 & 0 & N_5 & -N_6 \\ 0 & 0 & 0 & 0 & 0 & N_6 \end{bmatrix} \begin{bmatrix} i_1\\ i_2\\ i_3\\ i_4\\ i_5\\ i_6 \end{bmatrix} + \begin{bmatrix} 0\\ 0\\ 0\\ 0\\ 0\\ H_{pm}L_{pm} \end{bmatrix} \tag{30}$$

where

$$\Re_d = \frac{\sqrt{g_{0d}^2 - x_1^2 - x_2^2}}{(\mu_0 a_d)}. \tag{31}$$

The FTC requirements result in ten constraint equations

$$W^T\gamma_1 W = 0_{2\times 2} \tag{32}$$
$$2B_{\text{bias}}^T\gamma_1 W = [K_{v1}\ 0] \tag{33}$$
$$W^T\gamma_2 W = 0_{2\times 2} \tag{34}$$
$$2B_{\text{bias}}^T\gamma_2 W = [0\ K_{v2}]. \tag{35}$$

These equations are solved for t_{ij} and λ_k utilizing the Lagrange multiplier/nonlinear least square solver approach discussed for the six-pole HCB.

D. Decoupling Choke

The inductance matrix of the isolated combo bearing is singular because flux conservation introduces a dependency relation between the fluxes. This produces a potentially unstable operation state for the power amplifiers. Two decoupling chokes are added to the combo bearing according to Meeker's approach [2]. By adjusting the parameters of the decoupling chokes (N_{c1}, N_{c2}, N_{c3}, $\Re_{c1}$, $\Re_{c2}$), the inductance matrix becomes full rank and the mutual inductances become zero. Similarly, a single decoupling choke is added to the radial bearing.

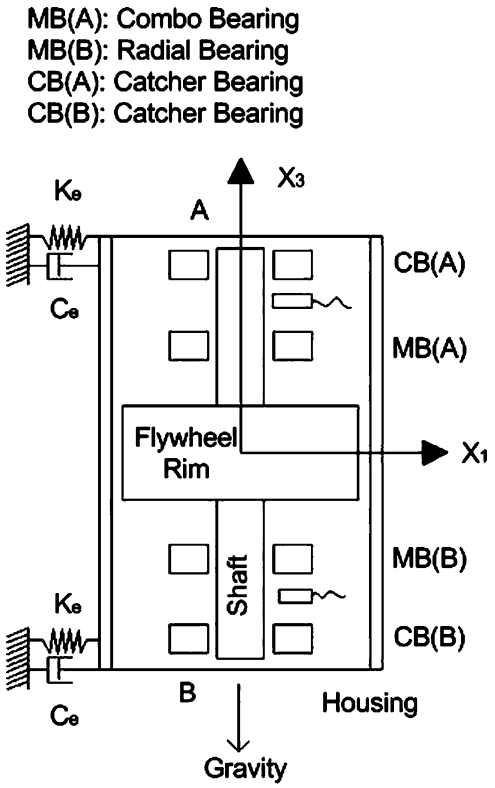

Fig. 4. Flywheel system with a magnetic suspension.

III. Flywheel and Magnetic Suspension Dynamics Model

The novel redundant actuators operate within a feedback-controlled system that includes both electrical component and structural component dynamics. A typical application is a flywheel module consisting of a high-speed shaft, integrally mounted motor-generator, composite flywheel rim, magnetic suspension, and flexibly mounted housing. Fig. 4 depicts a module model with nine rigid body structural degrees of freedom: rotor CG translations (X_{1r}, X_{2r}, X_{3r}), rotor rotations (θ_{1r}, θ_{2r}) housing CG translations (X_{1h}, X_{2h}), and housing rotation (θ_{1h}, θ_{2h}). The magnetic suspension employs magnetic (MB) and backup (catcher, CB) bearings at both the A and B ends of the module. Magnetic bearing clearances are approximately 0.5 mm, so small angle motion may be assumed. Let b, d, and c denote the magnetic actuator, mass imbalance, and catcher bearing forces, respectively. The equations of motion then become

$$\begin{bmatrix} M_r & 0 & 0 & 0 & 0 \\ 0 & I_{tr} & 0 & 0 & 0 \\ 0 & 0 & M_r & 0 & 0 \\ 0 & 0 & 0 & I_{tr} & 0 \\ 0 & 0 & 0 & 0 & M_r \end{bmatrix} \begin{bmatrix} \ddot{X}_{1r} \\ \ddot{\theta}_{1r} \\ \ddot{X}_{2r} \\ \ddot{\theta}_{2r} \\ \ddot{X}_{3r} \end{bmatrix} + \begin{bmatrix} 0 & 0 & 0 & 0 & 0 \\ 0 & 0 & 0 & I_{pr}\omega & 0 \\ 0 & 0 & 0 & 0 & 0 \\ 0 & -I_{pr}\omega & 0 & 0 & 0 \\ 0 & 0 & 0 & 0 & 0 \end{bmatrix} \begin{bmatrix} \dot{X}_{1r} \\ \dot{\theta}_{1r} \\ \dot{X}_{2r} \\ \dot{\theta}_{2r} \\ \dot{X}_{3r} \end{bmatrix}$$

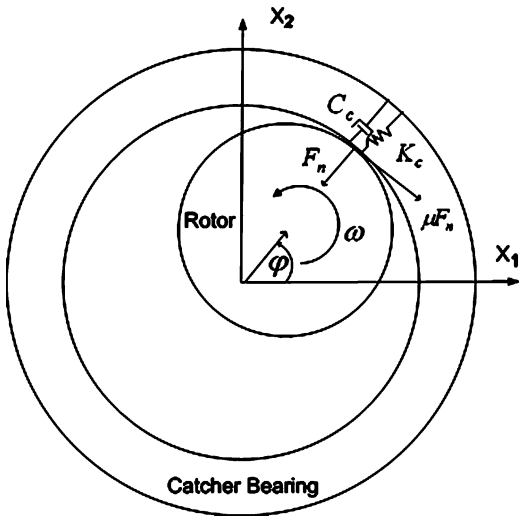

Fig. 5. Catcher bearing contact model.

$$= \begin{bmatrix} 1 & 0 & 0 & 1 & 0 \\ 0 & -L_{br}^{A} & 0 & 0 & L_{br}^{B} \\ 0 & 1 & 0 & 0 & 1 \\ L_{br}^{A} & 0 & 0 & -L_{br}^{B} & 0 \\ 0 & 0 & 1 & 0 & 0 \end{bmatrix} \begin{bmatrix} F_{1b}^{A} \\ F_{2b}^{A} \\ F_{3b}^{A} \\ F_{1b}^{B} \\ F_{2b}^{B} \end{bmatrix} + \begin{bmatrix} 1 & 0 & 0 & 1 & 0 \\ 0 & -L_{cr}^{A} & 0 & 0 & L_{cr}^{B} \\ 0 & 1 & 0 & 0 & 1 \\ L_{cr}^{A} & 0 & 0 & -L_{cr}^{B} & 0 \\ 0 & 0 & 1 & 0 & 0 \end{bmatrix} \begin{bmatrix} F_{1c}^{A} \\ F_{2c}^{A} \\ F_{3c}^{A} \\ F_{1c}^{B} \\ F_{2c}^{B} \end{bmatrix} + \begin{bmatrix} 1 & 0 & 0 & 1 & 0 \\ 0 & -L_{dr}^{A} & 0 & 0 & L_{dr}^{B} \\ 0 & 1 & 0 & 0 & 1 \\ L_{dr}^{A} & 0 & 0 & -L_{dr}^{B} & 0 \\ 0 & 0 & 1 & 0 & 0 \end{bmatrix} \begin{bmatrix} F_{1d}^{A} \\ F_{2d}^{A} \\ -M_r g \\ F_{1d}^{B} \\ F_{2d}^{B} \end{bmatrix} \tag{36}$$

$$\begin{bmatrix} M_h & 0 & 0 & 0 \\ 0 & I_{t1h} & 0 & 0 \\ 0 & 0 & M_h & 0 \\ 0 & 0 & 0 & I_{t2h} \end{bmatrix} \begin{bmatrix} \ddot{X}_{1h} \\ \ddot{\theta}_{1h} \\ \ddot{X}_{2h} \\ \ddot{\theta}_{2h} \end{bmatrix} + \begin{bmatrix} 2 & 0 & 0 & L_{eh}^{A} - L_{eh}^{B} \\ 0 & \left(L_{eh}^{A}\right)^2 + \left(L_{eh}^{B}\right)^2 & -L_{eh}^{A} + L_{eh}^{B} & 0 \\ 0 & -L_{eh}^{A} + L_{eh}^{B} & 2 & 0 \\ L_{eh}^{A} + L_{eh}^{B} & 0 & 0 & \left(L_{eh}^{A}\right)^2 + \left(L_{eh}^{B}\right)^2 \end{bmatrix} \times \left(C_e \begin{bmatrix} \dot{X}_{1h} \\ \dot{\theta}_{1h} \\ \dot{X}_{2h} \\ \dot{\theta}_{2h} \end{bmatrix} + K_e \begin{bmatrix} X_{1h} \\ \theta_{1h} \\ X_{2h} \\ \theta_{2h} \end{bmatrix} \right) = - \begin{bmatrix} 1 & 0 & 1 & 0 \\ 0 & -L_{bh}^{A} & 0 & L_{bh}^{B} \\ 0 & 1 & 0 & 1 \\ L_{bh}^{A} & 0 & -L_{bh}^{B} & 0 \end{bmatrix} \times \begin{bmatrix} F_{1b}^{A} \\ F_{2b}^{A} \\ F_{1b}^{B} \\ F_{2b}^{B} \end{bmatrix} - \begin{bmatrix} 1 & 0 & 1 & 0 \\ 0 & -L_{ch}^{A} & 0 & L_{ch}^{B} \\ 0 & 1 & 0 & 1 \\ L_{ch}^{A} & 0 & -L_{ch}^{B} & 0 \end{bmatrix} \begin{bmatrix} F_{1c}^{A} \\ F_{2c}^{A} \\ F_{1c}^{B} \\ F_{2c}^{B} \end{bmatrix}. \tag{37}$$

The nonlinear magnetic forces are determined by (16) and the catcher bearing model shown in Fig. 5 is employed for calculating the reaction forces when the rotor and catcher bearings contact. More sophisticated models with internal dynamics of races and balls or rollers are available [10] and could also be

TABLE I
FLYWHEEL MODEL PARAMETER LIST

Parameter	Value	Parameter	Value
M_r	29.644 (kg)	M_h	34.428 (kg)
I_{tr}	0.26233 (kg-m²)	I_{pr}	0.11129 (kg-m²)
I_{t1h}	1.5337 (kg-m²)	I_{t2h}	1.3993 (kg-m²)
K_e	3.5024E+5 (N/m)	C_e	5.2535E+3 (kg/s)
ϖ	60,000 (rpm)	e	8.4667E-7 (m)
L^A_{br}	0.14051 (m)	L^B_{br}	0.13360 (m)
L^A_{dr}	0.14051 (m)	L^B_{dr}	0.13360 (m)
L^A_{sr}	0.17846 (m)	L^B_{sr}	0.16974 (m)
L^A_{cr}	0.26765 (m)	L^B_{cr}	0.28067 (m)
L^A_{bh}	0.14051 (m)	L^B_{bh}	0.13360 (m)
L^A_{sh}	0.17856 (m)	L^B_{sh}	0.16974 (m)
L^A_{ch}	0.26765 (m)	L^B_{ck}	0.28067 (m)
L^A_{ek}	0.26765 (m)	L^B_{ek}	0.28067 (m)
ψ	$\pi/2$		

TABLE II
MAGNETIC BEARING PARAMETER LIST

Parameter	Combo Bearing	Radial Bearing
air gap	radial: 5.080E-4 (m) axial: 5.080E-4 (m)	Radial: 5.080E-4 (m) dead pole: 2 030E-3 (m)
radial pole face area	3.924E-4 (m²)	4.764E-4 (m²)
axial pole face area	1.719E-3 (m²)	N/A
dead pole face area	N/A	4.962E-3 (m²)
total face area of PM	3.178E-3 (m²)	3.844E-3 (m²)
length of PM	0.010 (m)	0.010 (m)
no. of turns of radial coil	24	24
no. of turns of axial coil	37	N/A
relative permeability of PM	1.055	1.055
coercive force of PM	950000 (A/m)	950000 (A/m)

used in the system dynamics model. The mass imbalance disturbance in the model is described by

$$F^A_{1d} = M_r e\omega^2 \cos\omega t \tag{38}$$
$$F^A_{2d} = M_r e\omega^2 \sin\omega t \tag{39}$$
$$F^B_{1d} = M_r e\omega^2 \cos(\omega t + \psi) \tag{40}$$
$$F^B_{2d} = M_r e\omega^2 \sin(\omega t + \psi). \tag{41}$$

IV. EXAMPLES

An example flywheel module illustrates operation and reliability of the redundant magnetic suspension. Table I lists the geometrical, inertia and stiffness parameters for the model. The catcher bearing contact model in Fig. 5 has a stiffness of 10^8 (N/m), a damping of 5000 N·s/m and a dynamic friction coefficient of 0.1. Table II shows the magnetic bearing parameters for the magnetic suspension model.

The control law utilized in the model is MIMO based and similar to the work of Okada [11] and Ahrens [12], [13]. Fig. 6 illustrates the overall feedback control loop for the magnetic suspension. Eight power amplifiers are utilized for the combo bearing and six power amplifiers for the radial bearing. Five displacement sensors measure the relative displacements between the rotor and housing. CDMs for the combo and radial bearings

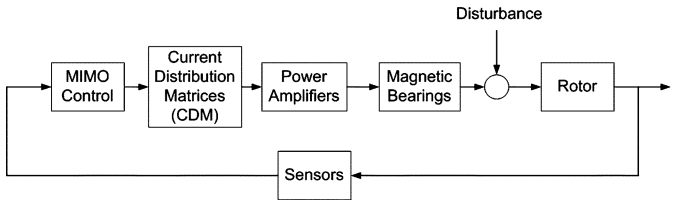

Fig. 6. Magnetic suspension control scheme.

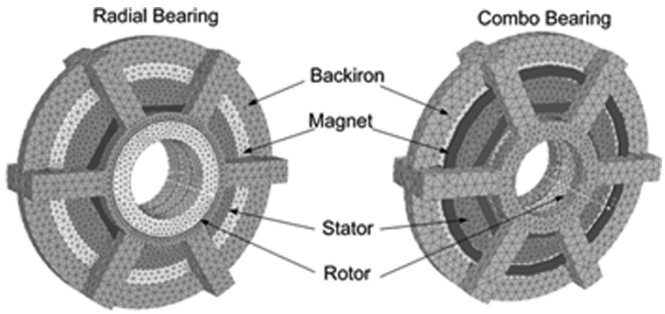

Fig. 7. 3-D FE model of the combo and radial six-pole actuators.

are incorporated in the controllers to produce reference voltages for the 14 power amplifiers which produce the desired currents in each coil.

The one-dimensional (1–D) magnetic circuit models as shown in Figs. 2 and 3 must be adjusted to include the effects of recirculation leakage of the flux between the N and S poles of any permanent magnet and for the effect of nonparallel (fringing) flux flow in the air gap of each pole. These effects are apparent in a three-dimensional (3–D) finite-element-based simulation of the actuator as shown in Fig. 7. These adjustments are made with multiplicative factors applied to the gap flux and permanent-magnetic coercive force in the 1-D model, as derived from the 3-D FE model. The permanent magnet coercive force is derated from 950 000 to 514 000 in the combo bearing and from 950 000 to 566 000 in the radial bearing. The air gap fluxes are derated with a fringe factor of 0.9 for both the combo and radial bearings.

The remaining parameters of the system model include displacement sensor sensitivity $= 7874$ V/m, displacement sensor bandwidth $= 5000$ Hz, power amplifier dc gain $= 1$ A/V, and power amplifier bandwidth $= 1200$ Hz.

These 3-D bearing models were also employed to verify the fault tolerant operation predicted with the 1-D model. An example of this is the three-pole failure results shown in Table III. The control voltage sets in this table are

$$V_c = (V_{c1}\ V_{c2}\ V_{c3})^T = \begin{cases} (1V\ 0\ 0)^T & \text{for set 1} \\ (0\ 1V\ 0)^T & \text{for set 2} \\ (0\ 0\ 1V)^T & \text{for set 3} \end{cases}. \tag{42}$$

The inductance matrix of the combo bearing with the two decoupling chokes is given in henries as

$$L_{CB} = 5.59 \times 10^{-4} \cdot \mathrm{diag}(1\ 1\ 1\ 1\ 1\ 1\ 10.43\ 10.43). \tag{43}$$

The inductance matrix of the radial bearing with a decoupling choke is given in henries as

$$L_{RB} = 6.76 \times 10^{-4} \cdot \mathrm{diag}(1\ 1\ 1\ 1\ 1\ 1). \tag{44}$$

TABLE III
1-D AND 3-D MODEL COMPARISON OF PREDICTED FORCES FOR SIX-POLE COMBO BEARING

Control Voltage Set	Force Direction	Force (N)			
		No Poles Failed		3 Poles Failed	
		1D Model	3D Model	1D Model	3D Model
1	X1	11.64	12.95	11.64	12.96
1	X2	0	0.01	-0.14	-0.25
1	X3	0	0.04	0	-0.03
2	X1	0	0.02	0	-0.08
2	X2	11.64	13.3	11.59	13.17
2	X3	0	0.08	0	-0.05
3	X1	0	-0.4	0	-0.4
3	X2	0	0.66	0	0.66
3	X3	8.9	9.4	8.9	9.4

The current produced by a power amplifier is turned off at the moment of failure which simulates an open circuit. This is implemented in the model by changing the K matrix in (9) from the identity matrix to its pole-failed value, while the no-pole failed CDM is retained. The appropriate CDM for the pole-failure configuration being tested is then swapped in following a delay time. The MIMO control law in Fig. 6 is invariant throughout the entire simulation. The combo and radial bearing CDMs for the no-pole failed state are

$$T_o^A = \begin{bmatrix} 0.307\,89 & 0.177\,76 & 0 \\ 0 & 0.355\,52 & 0 \\ -0.307\,89 & 0.177\,76 & 0 \\ -0.307\,89 & -0.177\,76 & 0 \\ 0 & -0.355\,52 & 0 \\ 0.307\,89 & -0.177\,76 & 0 \\ 0 & 0 & -0.115\,30 \\ 0 & 0 & 0.115\,30 \end{bmatrix}$$

$$T_o^B = \begin{bmatrix} 0.280\,74 & 0.162\,09 \\ 0 & 0.324\,17 \\ -0.280\,74 & 0.162\,09 \\ -0.280\,74 & -0.162\,09 \\ 0 & -0.324\,17 \\ 0.280\,74 & -0.162\,09 \end{bmatrix}.$$

The new CDMs for the poles 1-2 failed case in Fig. 1 are

$$T_{12}^A = \begin{bmatrix} 0 & 0 & 0 \\ 0 & 0 & 0 \\ -0.663\,89 & 0 & 0 \\ -0.230\,32 & -0.582\,96 & 0 \\ -0.385\,45 & -0.483\,60 & 0 \\ 0.337\,34 & -0.579\,34 & 0 \\ 0 & 0 & -0.115\,30 \\ 0 & 0 & 0.115\,30 \end{bmatrix}$$

$$T_{12}^B = \begin{bmatrix} 0 & 0 \\ 0 & 0 \\ -0.604\,75 & 0 \\ -0.211\,82 & -0.530\,41 \\ -0.349\,67 & -0.442\,11 \\ 0.306\,40 & -0.527\,69 \end{bmatrix}.$$

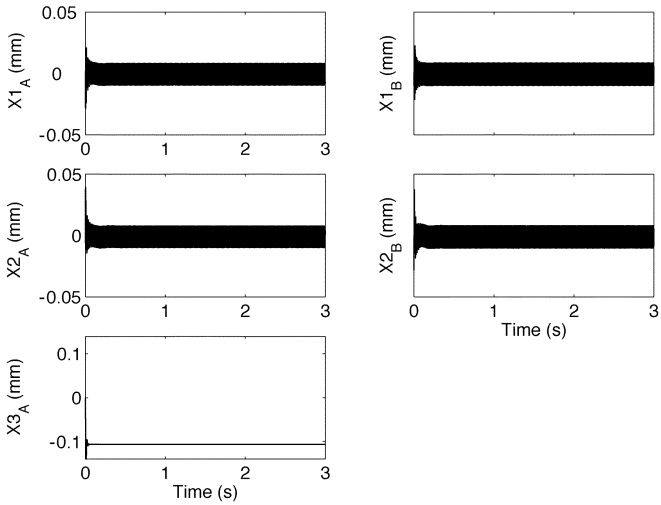

Fig. 8. Rotor displacements in the radial and axial direction for example 1.

The new CDMs for the poles 1-2-3-4 failed case in Fig. 1 are

$$T_{1234}^A = \begin{bmatrix} 0 & 0 & 0 \\ 0 & 0 & 0 \\ 0 & 0 & 0 \\ 0 & 0 & 0 \\ -0.607\,42 & -1.0622 & 0 \\ 1.2224 & -3.6408 \times 10^{-3} & 0 \\ 0 & 0 & -0.115\,30 \\ 0 & 0 & 0.115\,30 \end{bmatrix}$$

$$T_{1234}^B = \begin{bmatrix} 0 & 0 \\ 0 & 0 \\ 0 & 0 \\ 0 & 0 \\ -0.553\,79 & -0.968\,48 \\ 1.114\,60 & -3.3556 \times 10^{-3} \end{bmatrix}.$$

The text below discusses two illustrative examples that assume identical failures in both the radial and combo bearings. Although this represents a rare occurrence it serves to illustrate the method and analysis presented. Example 1 considers failing radial poles 1 and 2, and example 2 considers failing radial poles 1, 2, 3, and 4 in Fig. 1. Fig. 8 reveals that for example 1 excellent control is maintained utilizing the no-poles failed CDMs throughout the entire simulation. This example shows that the closed loop is still stable due to the partial actuator failure. The currents in the 14 amplifiers are shown in Figs. 9 and 10 for a failure initiation at 0.1 s. The currents of the failed PAs become zero, and the currents of the unfailed PAs are the same as before failure. Consequently, the no-poles failed CDMs satisfy the success criterion for the reliability and is independent of the delay time.

In contrast, the closed loop system of example 2 is not stable with partial actuator failure if the CDM is not swapped. The 1-2-3-4 poles failed CDMs (T_{1234}^A, T_{1234}^B) must be activated after delay time to maintain control invariance. The displacement, current, and flux responses for example 2 are shown in Figs. 11–15 for $\tau_d = 20$ ms and a failure initiation at 0.1 s. The displacements have transient responses due to the PA failure. However, they return to steady state after the new CDMs are activated. The currents of the failed PAs become zero after the failure, but the currents of the unfailed PAs increase due to the larger

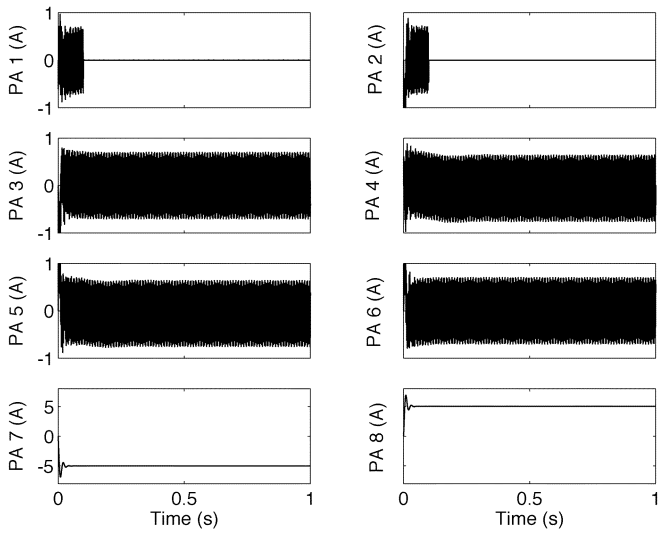

Fig. 9. Current responses in HCB for example 1.

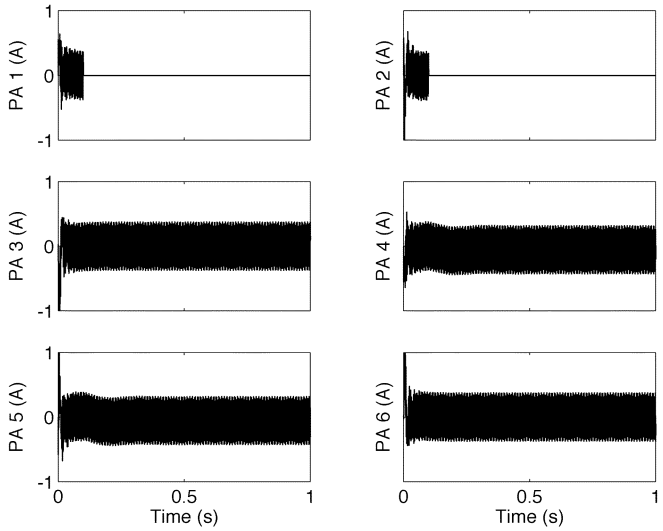

Fig. 10. Current responses in HRB for example 1.

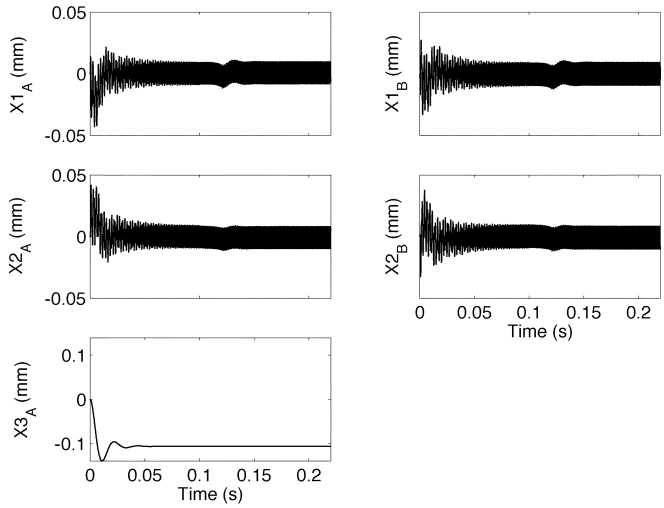

Fig. 11. Rotor displacements in the radial and axial direction for example 2.

Frobenius norms of the new CDMs. The bias flux density in the radial poles is around 0.7 T for the HRB and 0.72 T for the HCB. The control flux of the HCB is around 0.03 T (4% of the bias flux) before the failure and 0.1 T (14% of the bias flux) after the failure. The control flux of the HRB is around 0.015 T (2% of the bias flux) before the failure and 0.05 T (7% of the bias flux) after the failure. Consequently, the 1-2-3-4 poles failed CDMs satisfy the success criterion for reliability.

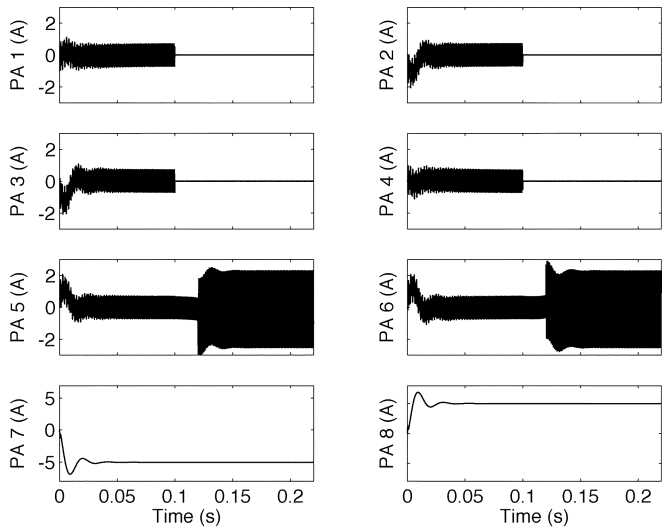

Fig. 12. Current responses in HCB for example 2.

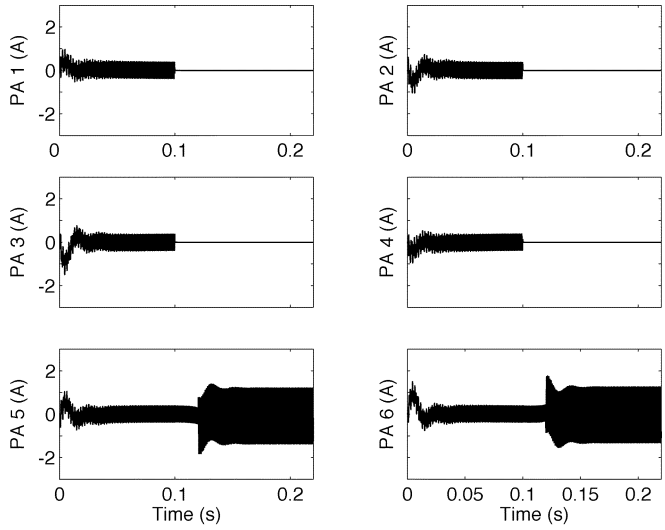

Fig. 13. Current responses in HRB for example 2.

When contacts between the rotor and the catcher bearings happen during swapping the CDMs, the rotor may be relevitated. Fig. 16 shows the displacements for a successful relevitation event with poles 1-2-3-4 failed, $\tau_d = 100$ ms, $\mu = 0.1$, $C_c = 5,000$ N $\cdot$ s/m, and $K_c = 10^8$ N/m. This is highly dependent on whether backward whirl develops during the contact period. The backward whirl state occurs due to friction at the contact interface between the shaft and the catcher bearings, which forces the shaft to whirl (precess) in a direction opposite to the spin direction. Fig. 17 shows an example of this state with $\mu = 0.3$, $C_c = 10^5$ N$\cdot$s/m, and $K_c = 10^8$ N/m. The backward whirl eccentricity is the catcher bearing clearance (typically 0.25 mm) for a rigid rotor, and possibly a much larger value for a flexible shaft. The whirl frequency typically

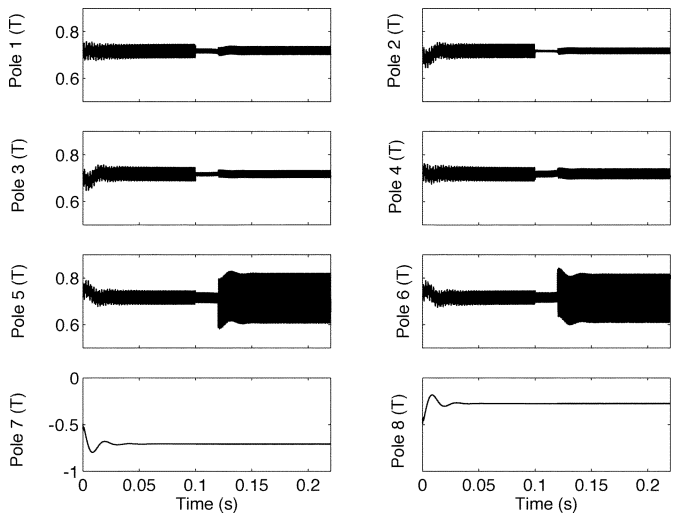

Fig. 14. Flux density responses in HCB for example 2.

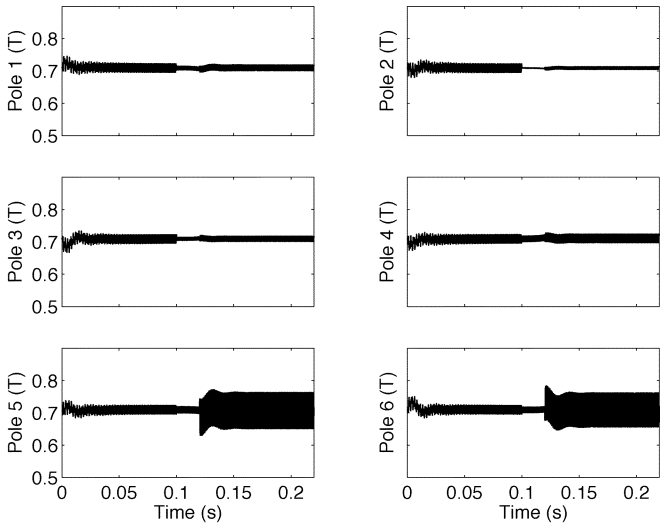

Fig. 15. Flux density responses in HRB for example 2.

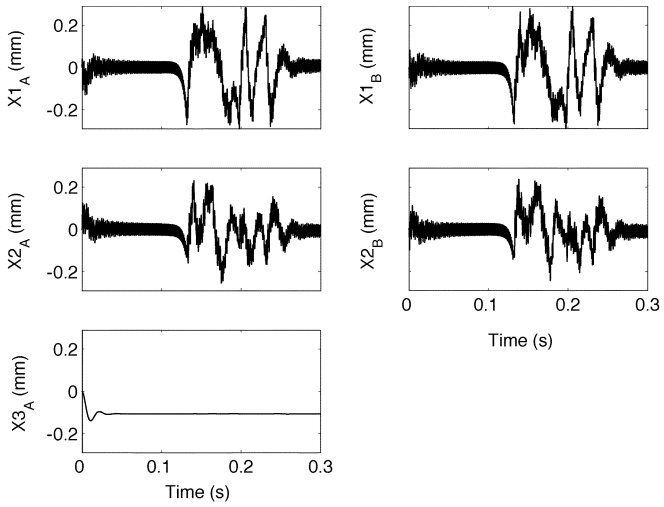

Fig. 16. Rotor displacements in the radial and axial direction during successful relevitation.

ranges from 0.4 to 1.0 times the spin frequency. This creates a potentially large centrifugal force that can damage the catcher bearings or deflect the shaft into the magnetic bearings. The backward whirl condition is mitigated by proper design of the flexible damped support, preload, clearance, and friction coefficient for the catcher bearings. Relevitation off of the catcher bearings is very difficult once backward whirl has fully developed.

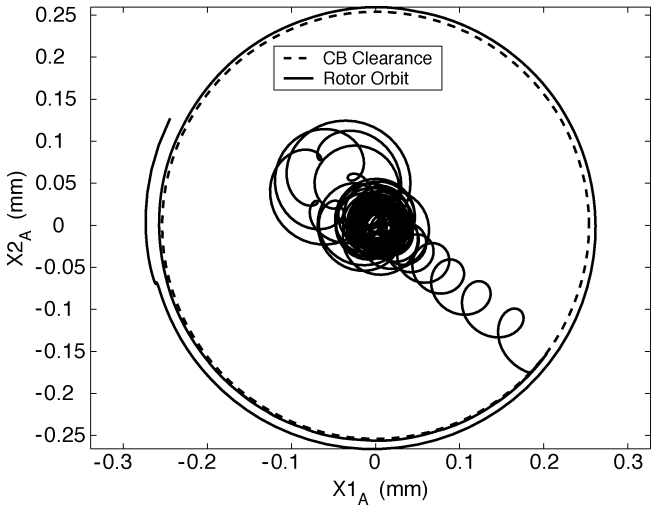

Fig. 17. Orbit plot of the rotor at CB(A).

V. Reliabilities of Magnetic Bearings

The reliability of a magnetic bearing is determined by considering the number of failed pole states that still meet the success criterion. This is dependent on the delay time, modeling assumptions, number of poles in the bearing, and the reliability of the power amplifier/coil units that drive and conduct the bearing currents. The four-pole and seven-pole configurations require two less or one more power amplifiers than the six-pole configuration, respectively. The radial pole and permanent-magnet cross-sectional areas, the number of turns of each radial coil, and the coercive force and the length of the permanent magnets for the four- and seven-pole bearings are identical to those of the six-pole bearing.

The no-pole failed CDMs for the seven-pole bearing are

$$T_o^A = \begin{bmatrix} 0.330\,71 & -0.017\,910 & -4.6780 \times 10^{-3} \\ 0.177\,99 & 0.266\,01 & 3.6330 \times 10^{-3} \\ -0.067\,428 & 0.263\,96 & -2.7850 \times 10^{-3} \\ -0.266\,76 & 0.161\,81 & 7.8561 \times 10^{-4} \\ -0.298\,80 & -0.155\,75 & 1.7079 \times 10^{-3} \\ -0.038\,458 & -0.292\,04 & -4.2590 \times 10^{-3} \\ 0.159\,65 & -0.238\,55 & 4.9591 \times 10^{-3} \\ 0 & 0 & -0.099\,552 \\ 0 & 0 & 0.099\,552 \end{bmatrix}$$

$$T_o^B = \begin{bmatrix} 0.284\,02 & 0 \\ 0.177\,08 & 0.222\,06 \\ -0.063\,201 & 0.276\,90 \\ -0.255\,89 & 0.123\,23 \\ -0.255\,89 & -0.123\,23 \\ -0.063\,201 & -0.276\,90 \\ 0.177\,08 & -0.222\,06 \end{bmatrix}.$$

TABLE IV
SUMMARY OF SIMULATION FOR RELIABILITY STUDY

No. of Pole	Failed Bearing	No. of unfailed Poles (q)	No. of Simulation (I_{nq})	Swapping CDM (α_k)	Non-Swapping CDM (α_k)
4	Radial	2	6	4	4
		3	4	4	4
		4	1	1	1
	Combo	2	6	4	4
		3	4	4	4
		4	1	1	1
6	Radial	2	15	12	0
		3	20	20	8
		4	15	15	12
		5	6	6	6
		6	1	1	1
	Combo	2	15	12	0
		3	20	20	8
		4	15	15	12
		5	6	6	6
		6	1	1	1
7	Radial	2	21	16	0
		3	35	33	0
		4	35	35	14
		5	21	21	21
		6	7	7	7
		7	1	1	1
	Combo	2	21	13	0
		3	35	28	2
		4	35	35	14
		5	21	21	20
		6	7	7	7
		7	1	1	1

The no-pole failed CDMs for the four-pole bearing are

$$T_o^A = \begin{bmatrix} 0.525\,50 & 0 & 0 \\ 0 & 0.525\,50 & 0 \\ -0.525\,50 & 0 & 0 \\ 0 & -0.525\,50 & 0 \\ 0 & 0 & -0.170\,43 \\ 0 & 0 & 0.170\,43 \end{bmatrix}$$

$$T_o^B = \begin{bmatrix} 0.465\,39 & -1.073\,19 \times 10^{-3} \\ 7.3028 \times 10^{-4} & 0.463\,71 \\ -0.464\,03 & -1.073\,19 \times 10^{-3} \\ 7.3028 \times 10^{-4} & -0.465\,71 \end{bmatrix}.$$

The radial pole failure simulations are conducted with the combo bearing operating in a no-pole failed state, and vice versa. Failure occurs at 0.1 s into the simulation and swapping in of the new CDM occurs at a delay time 20 ms later. The number of q unfailed pole cases for an n pole bearing is given by the formula

$$I_{nq} = \binom{n}{q} = \frac{n!}{q!(n-q)!}. \tag{45}$$

Table IV summarizes the results of these simulations for swapping in the appropriate poles-failed (new) CDM for the delay times 20 ms and for nonswapping CDMs. An n-pole, fail-safe, homopolar magnetic bearing is similar to a "m-out-of-n" system in a reliability model if stable control is maintained when at minimum m of the n poles (P.A. plus coil) are unfailed. Let R_p represent the reliability of a "pole," i.e. of the power amplifier plus its pole coil, at some specific point in its expected lifetime. Also assume that "poles" are identical and act independently. The system reliability then becomes

$$R_s = \sum_{k=m}^{n} \alpha_k R_p^k (1 - R_p)^{n-k} \tag{46}$$

where α_k are the number of cases that satisfy the success criterion. The integer m in (46) is the minimum number of unfailed poles that are required for the n pole bearing to successfully levitate the shaft. The (n, m) pairs determined in this example are (4,2), (6,2), and (7,2). Fig. 18 shows system reliability versus R_p plots for the four-, six-, and seven-pole HRBs by swapping CDMs approach and for the two-axis MB without redundant design, i.e., if one of the two PAs fails, the MB fails. The HRB reliability is improved by increasing the number of radial poles and by the swapping CDMs approach even if R_p is decreasing according to the lifetime distribution. Similarly, Fig. 19 is for the nonswapping CDM approach (maintain the no-poles failed CDMs). The reliabilities of HRBs are higher than that of the

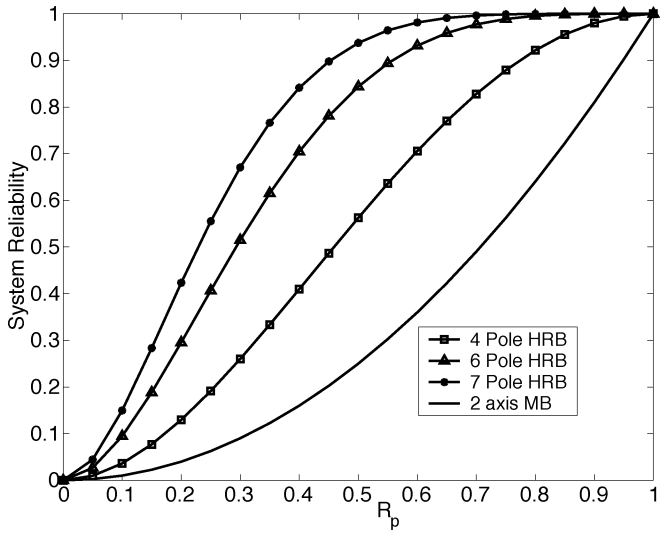

Fig. 18. System reliabilities of four-, six-, and seven-pole radial bearings for swapping CDMs.

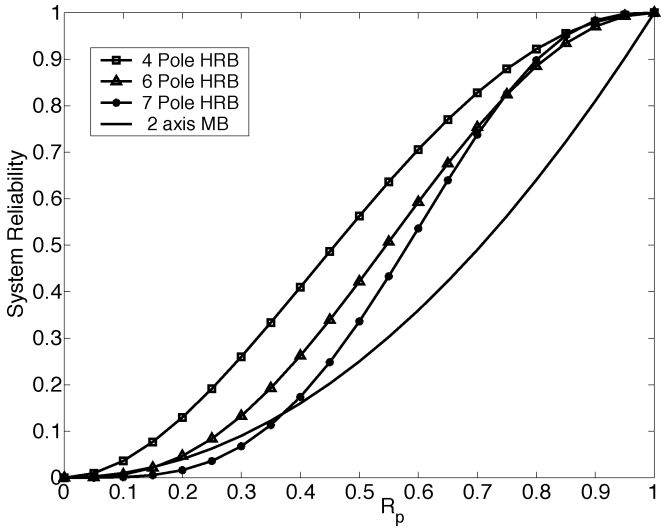

Fig. 19. System reliabilities of four-, six-, and seven-pole radial bearings for nonswapping CDMs.

two-axis MB when R_p is greater than 0.4. Increasing the number of poles does not imply higher system reliability if the CDMs are not swapped. The reliability of the swapping CDMs approach is better than the nonswapping approach. Consequently, the HCBs have the same trend as HRBs have.

VI. Conclusion

This paper presents a description, analysis, example, and reliability study for novel, redundant, radial and combination, homopolar magnetic bearings. Current distribution matrices are evaluated based on the set of poles that have failed and the requirements for uncoupled force/voltage control, linearity and specified force/voltage gains to be unaffected by the failure. The CDM algorithm also determines the CDM with a minimum Frobenius norm which provides reduced effort (current required) operation of the HOMB. The first advantage of the HOMB over a HEMB is the automatic invariance of the position stiffness before and after pole failure, and the second advantage is the high efficiency since the bias flux of HOMB is supplied by permanent magnets. The fault-tolerant control of the HEMBs by Na and Palazzolo [5] has high system reliability also since they demonstrated the successful operation of five pole failures out of eight poles.

A simplified catcher bearing model is employed to evaluate the relevitation after catcher bearing contact.

The numerical example presented exhibits several interesting trends, which include:

- the reliability of the four-, six-, or seven-pole bearing is high even if the reliability of the pole decreases with time;
- increased reliability with increased number of poles by swapping CDMs;
- successful levitation with only two unfailed poles for the $n = 4, 6$, and 7 pole HOMBs;
- successful fault-tolerant operation without changes to the MIMO control law.

Future work includes tests of six-pole radial and combination HOMBs in the G2-ACESE flywheel module at NASA Glenn. This will provide a means to correlate the theory presented here with test results. The tests are scheduled for early in 2005 and the correlation will be reported in a separate paper shortly thereafter. Finally, the MIMO control will also be modified to improve the reliability of operation without replacing the no-poles failed CDM with a pole-failed CDM.

Acknowledgment

The authors specifically thank K. McLallin, J. Soder, and J. Dudenhoefer of NASA Glenn, and F. Best and F. Little of the Texas A&M CSP for their administration of these programs.

References

[1] S. Iwaki, "The optimal location of electromagnets in multiple degree of freedom magnetically suspended actuators," *ASME J. Dyn. Syst., Meas. Contr.*, vol. 112, pp. 690–695, Dec. 1990.

[2] D. C. Meeker, "Optimal solution to the inverse problem in quadratic magnetic actuators," Ph.D. dissertation, Univ. Virginia, 1996.

[3] E. H. Maslen and D. C. Meeker, "Fault tolerance of magnetic bearings by generalized bias current linearization," *IEEE Trans. Magn.*, vol. 31, pp. 2304–2314, May 1995.

[4] E. H. Maslen, C. K. Sortore, and G. T. Gillies, "Fault tolerant magnetic bearings," *ASME J. Eng. Gas Turbines Power*, vol. 121, pp. 504–508, July 1999.

[5] U. J. Na and A. Palazzolo, "Optimized realization of fault-tolerant heteropolar magnetic bearings," *ASME J. Vib. Acoust.*, vol. 122, pp. 209–221, July 2000.

[6] U. J. Na, A. Palazzolo, and A. Provenza, "Test and theory correlation study for a flexible rotor on fault-tolerant magnetic bearings," *ASME J. Vib. Acoust.*, vol. 124, pp. 359–366, July 2002.

[7] U. J. Na and A. Palazzolo, "Fault tolerance of magnetic bearings with material path reluctances and fringing factors," *IEEE Trans. Magn.*, vol. 36, pp. 3939–3946, Nov. 2000.

[8] E. H. Maslen, P. E. Allaire, M. D. Noh, and C. K. Sortore, "Magnetic bearing design for reduced power consumption," *ASME J. Tribol.*, vol. 118, pp. 839–846, Oct. 1996.

[9] S. Skogestad and I. Postlethwaite, *Multivariable Feedback Control*. New York: Wiley, 1996, p. 519.

[10] G. Sun and A. B. Palazzolo, "Detailed bearing model for magnetic suspension auxiliary service," *J. Sound Vib.*, vol. 269, pp. 933–963, Jan. 2004.

[11] Y. Okada, B. Nagai, and T. Shimane, "Cross feedback stabilization of the digitally controlled magnetic bearing," *ASME J. Vib. Acoust.*, vol. 114, pp. 54–59, Jan. 1992.

[12] M. Ahrens, A. Traxler, P. Von Burg, and G. Schweitzer, "Design of a magnetically suspended flywheel energy storage device," in *Proc. 4th Int. Symp. Magnetic Bearings*, 1994, pp. 553–558.

[13] M. Ahrens, L. Kucera, and R. Larsonneur, "Performance of a magnetically suspended flywheel energy storage device," *IEEE Trans. Contr. Syst. Technol.*, vol. 4, pp. 494–502, Sept. 1996.